JOURNAL OF CATALYSIS 130, 332–346 (1991)

Electron Spectroscopic Studies of Mo- and Pt-Modified γ-Al_2O_3 Model Catalysts

A. JIMÉNEZ-GONZÁLEZ AND D. SCHMEISSER

Institut für Physikalische und Theoretische Chemie, Universität Tübingen, Auf der Morgenstelle 8, 7400 Tübingen, Germany

Received July 26, 1990; revised February 7, 1991

Model catalysts based on γ-Al_2O_3, prepared by oxidizing Al foils and thin films, are chemically modified by Mo and Pt. Electron spectroscopies reveal the chemical states of Mo and Pt depending on the treatment in oxidizing, reducing, and sulfidizing atmospheres. We find Mo to exist in the oxidation states 4+, 5+, and 6+, whereas Pt appears as Pt^0 and Pt^{2+}. For Pt-modified films agglomerates of a mixed Pt–Al oxide grow beside large areas which are free of Pt. The surface morphology of the Mo-modified films is found to depend on the Mo concentration. For the reduced and sulfided state a phase transition due to concentration-dependent occupation of tetrahedral and octahedral aluminum defect sites by Mo is followed, whereas at low Mo concentrations a homogeneous distribution can be deduced. © 1991 Academic Press, Inc.

1. INTRODUCTION

Spectroscopic methods are used in the investigation of catalysts to obtain information on the catalytic reaction mechanisms (*1, 2*), on the catalyst surface structure (*3, 4*), and on the influence of the support-metal interaction (*5*). For all of these studies, the characterization and the modification of the supports are also of importance. In particular for alumina-supported Mo and Pt catalysts, the γ-modification itself has a high catalytic activity when compared to the various other modifications of Al_2O_3. The Mo and Pt model catalysts studies in this work are aimed to simulate the catalysts used for hydrodesulfurization of fossil mineral oil products and exhaust-combustion reactions. The intermediate states of these catalysts which are obtained after oxidizing, reducing, and sulfurizing procedures are studied also.

The particular interaction of Mo with γ-Al_2O_3 is strongly correlated with the defect structure of γ-Al_2O_3. The aluminum cation is known to exist in both tetrahedral and octahedral coordination in the defect-rich spinel structure of γ-Al_2O_3. Although these coordinations have distinct differences they are similar when understood to arise from OH groups at different sites, confirmed by Raman and IR data (*3*). (110)-oriented γ-Al_2O_3 crystallites are stacked in alternating A and B slabs. The first slab contains both octahedral and tetrahedral cation vacancies, whereas the second slab has octahedral coordinated defects only.

Several electron, ion, and photon spectroscopies have been used for the characterization of Mo and Pt catalytic systems (*5–8*). XPS is used in catalysis as a tool to determine the oxidation state of transition metals. Pressed powders of γ-Al_2O_3 (*3, 9*), as well as the chemically modified supports of MoO_3/γ-Al_2O_3 and Pt/γ-Al_2O_3 have been studied intensively (*10–12*). Using electron and ion spectroscopic techniques, problems often arise for absolute and reproducible measurements, as both catalyst and support are highly insulating materials and an electric charge is built up during the experiment. This charge influences all energy levels derived from the sample, in particular for X-ray and UV-induced photoelectron (XPS, UPS), Auger electron (AES), ion scattering (ISS), and electron energy loss

0021-9517/91 $3.00

(ELS) spectroscopies. The use of a flood gun or a reference signal, for example Au 4*f* or C 1*s*, is often employed to correct for the charging. However, these corrections are not reliable because of the large errors arising from chemical interactions and by electron-induced variations, in the Au/γ-Al_2O_3 system or by adsorbed hydrocarbons, respectively.

In contrast, thin films do permit a spectroscopic characterization of γ-Al_2O_3 (*13*) by XPS, UPS, and ISS. Even valence band studies, determination of the work function, and the electron affinity as well as their temperature-dependent variations (*14*) are enabled. Using such model supports for studies of catalytic processes, we must consider several differences against real catalysts. Thin films of γ-Al_2O_3 certainly have surface properties different from those of γ-Al_2O_3 powders. Specific surface areas of the order of 200 m^2/g for the latter contrast with those around 1 m^2/g for the former. Further, the electrochemical activity for the oxygen ions is not known; in particular, it is not stabilized by a reference level and may differ significantly in γ-Al_2O_3 powders. The latter restriction is certainly severe, and all the conclusions drawn from our results are only valid under the assumption of a constant oxygen activity. Nevertheless, our data certainly give more information than previous studies which are influenced by charging effects. Also, the particular interaction of Pt and Mo toward γ-Al_2O_3 can be described adequately by the techniques employed.

In this work we have used γ-Al_2O_3 thin films with surfaces chemically modified by heat treatments in oxidizing, reducing, and sulfiding atmospheres. We have established that the crystal structure after these treatments is not altered and have determined the surface oxidation states of Mo and Pt by XPS with high accuracy. Thereby we are able to distinguish preparations which exhibit Mo in the (+V) state, which is believed to be responsible for the catalytic activity, whereas the stable MoO_2 and Mo_2O_3 oxides are not active. We also study the surface composition and variations in the Mo surface concentrations as revealed by XPS and ISS. The observed data are summarized in a model regarding chemical and geometric aspects of the active surface sites.

2. EXPERIMENTAL

Pure aluminum foils (99.9999%) are used for the preparation of thin films of γ-Al_2O_3 and are thermally oxidized in water vapor (4×10^{-3} mbar, 35 min) at different temperatures. Under such conditions a thin film grows of well-defined γ-Al_2O_3 grains, as described in detail in Ref. (*13*). For the preparation of chemically modified MoO_3/γ-Al_2O_3, as prepared thin films of γ-Al_2O_3 are dipped in an aqueous ammonium–heptamolybdate–tetrahydrate solution, or an aqueous hexachloroplatinum(IV)-acid–hexahydrate solution for the Pt/γ-Al_2O_3 catalyst. The concentrations and handling procedures of the adsorbed metals used are close to the parameters of technical catalysts; a detailed description of the preparation parameters is given in Ref. (*13*). After the impregnation, the samples are transferred to the UHV system within 10 min and are characterized by electron spectroscopies. To obtain the oxidized state of the catalysts, the modified films are heated in oxygen (200 mbar, 2 h) at 500°C. Afterward, the catalysts are reduced in hydrogen (100 mbar, 2 h) at 500°C to obtain the reduced state. For the MoO_3/γ-Al_2O_3 system, after the reduced state the catalyst is sulfided in a H_2S atmosphere (2 mbar, 1 h) at 400°C.

The experimental setup for the spectroscopic measurements, high-pressure cells, and transfer systems are described elsewhere (*13, 15, 16*). The XPS spectra are recorded using a Leybold–Heraeus spectrometer and Mg$K\alpha$ excitation. The spectrometer is calibrated against the core levels of metal foils, such as Al 2*p* at 73.2 eV and Mo $3d_{5/2}$ at 228.3 eV (*17*). The smoothed and background-subtracted emission patterns of the Mo 3*d* levels are decomposed into one or more doublets of Gaussians using a mathematical fitting procedure (*18*).

The concentration (atomic percentage) of molybdenum for the chemically modified thin films of γ-Al_2O_3 is determined by the relative intensities of the Al 2*p*, Mo 3*d*, O 1*s*, and S 2*p* levels as well as their sensitivity factors toward the LH-analyser.

Low-energy ion scattering spectroscopy (LEISS) was performed at a fixed scattering angle of 135° using 1 keV He^+ ions. Secondary electron micrography (SEM), Auger electron spectra (AES), and energy dispersive analysis by X-rays (EDX) were recorded using a Perkin–Elmer Φ600 spectrometer equipped with a windowless Tracor Northern X-ray detector. The samples are prepared in the UHV system described above and the SAES/EDX spectra are taken after transferring the sample through air. The studies using a transmission electron microscope (TEM) are performed in a Philips EM420 instrument. The MoO_3/γ-Al_2O_3 films are separated from the aluminum support using an aqueous solution of mercury chloride.

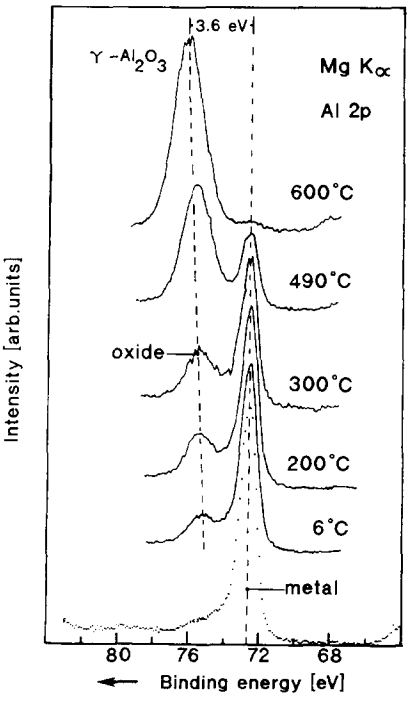

FIG. 1. Al 2*p* photoemission spectra of aluminum oxide during aluminum oxidation with water vapor at different support temperatures.

3. RESULTS

3.1 Thin Films of γ-Al_2O_3

The growth mechanism of γ-Al_2O_3 can be followed by XPS. Metallic aluminum has been oxidized in water vapor to reach saturation. Oxides obtained at different support temperatures show characteristic shifts of the Al 2*p* emission with respect to the metallic signal (Fig. 1). These core-level shifts, as displayed versus the support temperature in Fig. 2a, increase with increasing temperature from 2.6 to 3.6 eV and are used to identify different phases of Al_2O_3. For temperature below 300°C we find a core-level shift of 2.6 eV which can be assigned to an amorphous Al_2O_3, according to earlier XPS data (*19–22*). This assignment is in agreement with the Al–O phase diagram, in which at such temperatures several aluminum hydroxides are formed due to the interaction with water vapor. The transition to γ-Al_2O_3 occurs above 400°C (*9*), and we find an increase in the shift of the core levels up to 3.6 eV. This enormous difference allows us to distinguish between amorphous alumina and the γ-phase, and thereby an easy characterization of these different Al_2O_3 modifications by XPS is possible.

The crystal structure of γ-Al_2O_3 films was determined using transmission electron microscopy. In Fig. 2 (bottom) we show the TEM picture of a film oxidized in water vapor (4×10^{-3} mbar, 35 min) at 600°C. For as prepared films, we observe grains of γ-Al_2O_3 with an average diameter of 0.2 μm. The structure of these grains can be determined from the diffraction pattern which shows the [110] plane of the γ-Al_2O_3 crystal structure. The *y* modification is evident from the determination of the lattice constant (*13*). The identification of the most intense diffraction spots is given in Fig. 2.

These results demonstrate that we have succeeded in preparing γ-Al_2O_3 films and have characterized their structure by TEM and by XPS. In the following we concentrate on investigations of thin films of γ-Al_2O_3

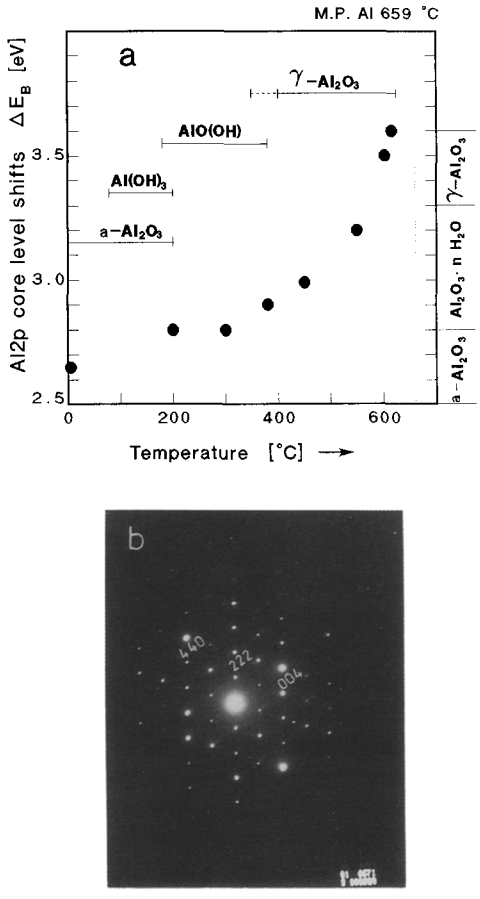

FIG. 2. (a) Al 2*p* core level shifts dependent on the support temperature (6–600°C) during the thermal oxidation of aluminum in water vapor. (b) TEM diffraction pattern of γ-Al_2O_3 thin films prepared at 600°C. The crystal orientation is along the [110] direction.

prepared at 600°C in water vapor with thicknesses in the range of 500 Å.

3.2 Chemical States of MoO_3/γ-Al_2O_3

After *impregnation* of the γ-Al_2O_3 thin films with molybdenum oxide, the Mo 3*d* spectrum of the modified γ-Al_2O_3 system is shown in Fig. 3A and compared to the metallic Mo 3*d* doublet (bottom curve). We observe significant core-level shifts, and not a sharp Mo 3*d* structure but rather a pattern which consists of several contributions. The binding energy E_B^F at maximum emission is 233.1 eV. When referred to the valence band maximum the binding energy of the Mo $3d_{5/2}$ level is 277.5 eV.

In the *oxidized state* of the modified MoO_3/γ-Al_2O_3 system we observe clearly separated Mo 3*d* core levels (3.2 eV spin-orbit splitting), as shown in Figs. 3B and 3C for two different molybdenum concentrations. We find a single doublet for the Mo 3*d* levels at 228.7 eV (Mo $3d_{5/2}$) for all Mo concentrations investigated. The FWHM is almost independent on the Mo concentra-

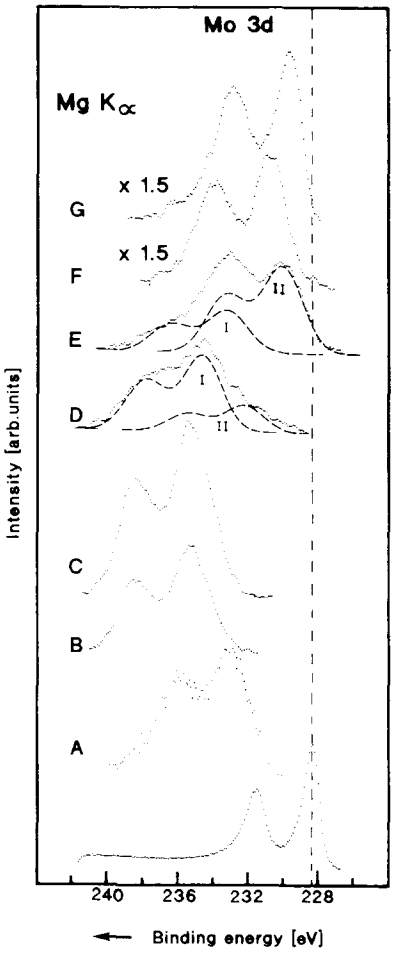

FIG. 3. XPS measurements of Mo 3*d* levels for chemically modified γ-Al_2O_3 supports (A) after impregnation of Mo, (B) after oxidation (5.0%), and (C) (7.0%), (D) after reduction (4.37%), and (E) (7.03%), (F) after sulfurization (3.02%), and (G) (6.22%). The Mo 3*d* levels of a Mo foil are given as reference (bottom curve).

tion and is around 2.5 eV. These findings indicate that in the oxidized state of MoO_3/γ-Al_2O_3, for all Mo concentrations we obtain a single oxidation state.

In the *reduced state* the Mo 3*d* levels change both their profile and their binding energies. The binding energy is reduced and the peak form corresponds no longer to a single doublet. At higher molybdenum concentrations the peak width is considerably increased, and shifted toward lower binding energies. Using a procedure that separates the range of the Mo 3*d* levels into doublets of Gaussians, we note that only two doublets are necessary to obtain a reasonable fit. Thereby, the high binding energy side is used to determine the amount of Mo(VI), whereas the low binding energy side can be used to distinguish between contributions of Mo(V) and Mo(IV). For the two different Mo concentrations shown in Fig. 3D und 3E the analyzed curves are included (dashed lines). The energy positions of their relevant spin-orbit signals are given in Table 1. We note that the relative intensities of the Mo 3*d* signals as well as their energy positions change by variation of the Mo concentration, and the FWHM in both doublets is increased up to 2.7 eV.

In the *sulfidized state* of the MoO_3/γ-Al_2O_3 system the Mo 3*d* photoemission spectra are shown for two different Mo concentrations as curves 3F and 3G. The Mo 3*d* emission pattern shifts further to lower binding energies (see also Table 1); for higher Mo concentrations the spectra resemble the stabilization of a single oxidation state doublet with a FWHM of 2.4 eV.

In all modification states we have also investigated the surface composition using the extreme surface sensitivity of LEISS. Figure 4 represents the spectra of the clean γ-Al_2O_3 state (A), after molybdenum impregnation (B), in the oxidized state (C), the reduced state (D), and in the sulfided state (E). We observe strong variations of the relative intensities dependent on the pretreatment of the sample. The O/Al ratio for the bare γ-Al_2O_3 films is 0.9, it increases after impregnation to 1.0, and after oxidation to 1.1. Also, the Al/Mo ratio increases from 4.9 to 6.1. Reduction causes a change of these ratios to 0.85 and 8.1, respectively. Further, we note that the relative intensities are not stable upon annealing; rather we observe a redistribution of the surface atoms as, for example, for a sample with 4.4% Mo (XPS) in the reduced state the O/Al ratio decreases from 0.8 to 0.7 at 338°C and the

TABLE 1

The Relative Occupation of the Different Oxidation States of Mo (Binding Energies Referred to the Valence Band Maximum E_B^V in eV, Rel. Percentage in %) are Given for Different Mo Concentrations

Mo content (At.%)	Oxidized state Mo $3d_{5/2}$ (VI) (eV)				FWHM (eV)
7.0	228.7 (235.8)				2.40
5.9	228.7 (235.8)				2.50
5.4	228.7 (235.8)				2.55
5.4	228.8 (235.9)				2.55
	Reduced state				
Mo content (At.%)	Mo $3d_{5/2}$ (I) Pos.(eV)	(%)	Mo $3d_{5/2}$ (II) Pos.(eV)	(%)	FWHM (eV)
7.0	225.9 (233.1)	36	222.7 (230.0)	63	2.70
4.4	227.7 (234.2)	40	224.4 (231.3)	59	2.60
4.3	227.6 (234.5)	69	225.2 (232.1)	30	2.70
1.3	227.5 (234.4)	84	224.5 (231.4)	15	2.65
	Sulfurized state				
Mo content (At.%)	Mo $3d_{5/2}$ (I) Pos.(eV)	(%)	Mo $3d_{5/2}$ (II) Pos.(eV)	(%)	FWHM (eV)
6.2	225.4 (232.8)	17	222.4 (229.8)	83	2.40
3.9	226.6 (233.7)	16	223.7 (230.8)	83	2.40
3.0	226.7 (233.8)	18	223.7 (230.8)	81	2.50
1.8	226.7 (233.8)	26	224.2 (231.3)	73	2.50

Note. The data in parentheses describe the binding energies with respect to E_B^F.

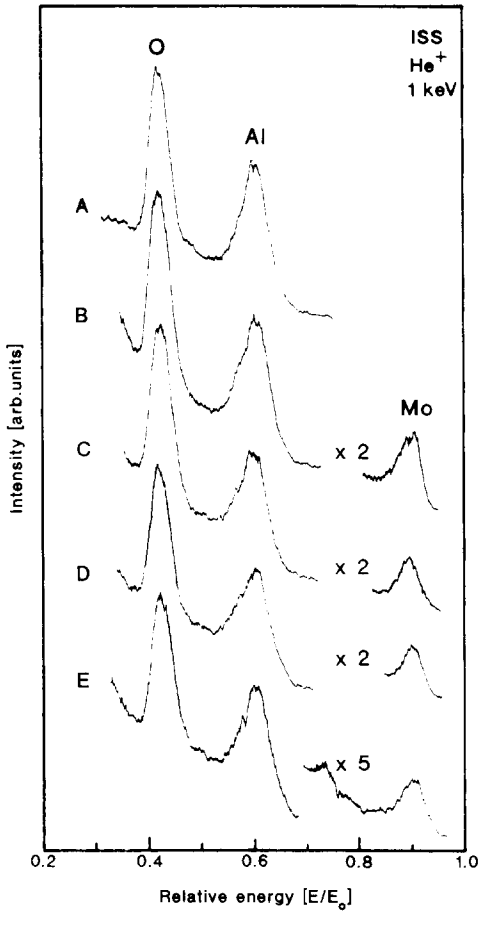

FIG. 4. Ion backscattering spectra (He^+, 1 keV) of (A) γ-Al_2O_3, (B) after impregnation by Mo, (C) MoO_3/γ-Al_2O_3 in the oxidized state, (D) MoO_3/γ-Al_2O_3 in the reduced state, (E) MoO_3/γ-Al_2O_3 in the sulfided state.

Al/Mo ratio from 8.2 to 6.2. The complete list of the relative intensity ratios is given in Table 2.

All chemical states (oxidized, reduced, and sulfided) of the modified γ-Al_2O_3 system with molybdenum oxide show no changes of the grain size and distribution in the TEM studies. Also, the crystal structure of the γ-Al_2O_3 film is not influenced by the various treatments as we find the same lattice parameters.

3.3 The System Pt/γ-Al_2O_3

The binding energies of the Pt 4*f* levels can be used as a reference for the chemical changes of platinum in the systenm Pt/γ-Al_2O_3 by comparison with those of metallic Pt (Curve B in Fig. 5). After the platinum impregnation the oxidized sample (100 mbar O_2, 2 h at 500°C) (Curve D in Fig. 5) shows a shift of the Pt 4*f* level to higher binding energies. Additional heat treatment in H_2 causes a broadening of the Pt levels and a shift toward lower binding energies.

Figure 6 shows the surface morphology of Pt/γ-Al_2O_3. Figure 6a is a photograph of a typical surface segment with a magnification of 204× and Fig. 6b with a 1000× magnification. We find that the samples show large agglomerates (C) on a smooth back-

TABLE 2

The Atomic Percentages of O, Al, Mo, and Their Ratios, as Determined from the XPS and the ISS Spectra, Respectively

O	Al	Mo	O/Al	O/Mo	Al/Mo
		Impregnation			
45	45	9	0.9	4.9	4.9
58	32	8			
47	44	8	1.0	5.4	5.1
60	35	4			
		Oxidized state			
47	41	11	1.1	4.1	3.58
57	36	6			
60	22	17	2.5	3.4	1.2
60	34	5			
49	43	7	1.1	7.0	6.1
58	36	5			
		Reduced state			
43	50	6	0.8	7.0	8.1
57	37	4			
42	52	5	0.8	8.3	10.1
57	37	4			
50	41	9	1.2	6.4	5.2
60	35	6			
		Sulfurized state			
43	52	4	0.8	10.8	12.1
60	35	4			

Note. The data are given for several samples after impregnation, and in the oxidized, reduced and sulfurized states at room temperature. The first line describes ISS data and the second the corresponding XPS data.

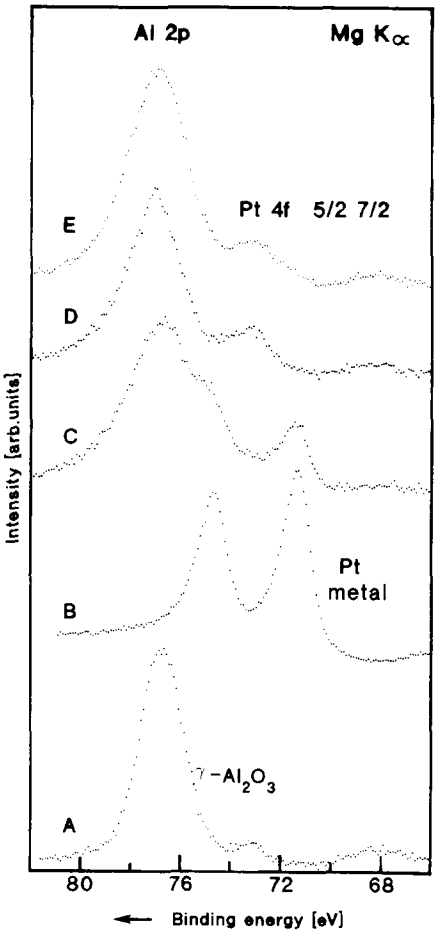

FIG. 5. Al 2*p* and Pt 4*f* photoemission spectra of Pt/γ-Al_2O_3 (A) The Al 2*p* emission of pure γ-Al_2O_3 (B) shows the metallic Pt 4*f* levels for reference (C) after Pt impregnation (D) after oxidation at 500°C and 100 mbar O_2.

ground (B), their size varying between 1 and 50 μm. To identify the elemental composition of these agglomerates we have used scanning AES. In Fig. 7 we show a direct comparison of Auger spectra taken at the background (B) and at the agglomerate (C). We find that the background (Fig. 7a) is composed of Al, O, and C, and within the experimental uncertainties it consists of γ-Al_2O_3 without Pt. On the other hand, we find that the large agglomerates (Fig. 7b) are composed of Pt, Al, O, and C.

AES is a method with high surface sensitivity, and therefore the spectra suffer considerably from carbon contaminations which arise from the transfer through air. More conclusive information, however, can be obtained using EDX which is a bulk sensitive method. In Fig. 8 the corresponding EDX spectra of the background (B) and of a cluster (C) are shown. We observe no Pt in the volume of the background (Fig. 8a), but we find considerable amounts of Pt in the bulk of the large agglomerates. This comparison of AES and EDX data is indicative of Pt diffusion into the bulk of γ-Al_2O_3 at the large agglomerates (Fig. 8b), and the formation of a mixed oxide.

4. DISCUSSION

The γ-modification of Al_2O_3 is found to be stable for the thin films prepared and investigated in this work. Its stability is demonstrated against heat treatment up to 620°C, in O_2, H_2O, or air (*13*). The stability is also demonstrated after the chemical modification with molybdenum and after different heat treatments in atmospheres of H_2, H_2S, and O_2, and air. This statement is made possible by recording the binding energies of the Al 2*p* levels after the various treatments. We find that the Al 2*p* emission from the γ-Al_2O_3 appears reproducible around 76.7 eV ($\pm$ 0.1 eV) which according to Fig. 1 can be used to monitor the stability of the γ-phase of Al_2O_3. Therefore, we conclude that none of the chemical modifications and heat treatments in H_2, H_2S, and O_2 affect the modification of the γ-Al_2O_3 support. Independently, we have used TEM after the treatments described and find no significant deviations from the patterns shown in Fig. 2b, i.e., there are no structural changes induced.

The binding state of Pt 4*f* varies after the oxidizing and reducing treatments. Starting with the initial preparation procedure, we observe almost pure, metallic Pt^0. In this case, Pt is reduced by interacting with aluminum. This reflects the noble character of Pt as, in comparison, Mo is found in the 4+ and 5+ oxidation states after similar

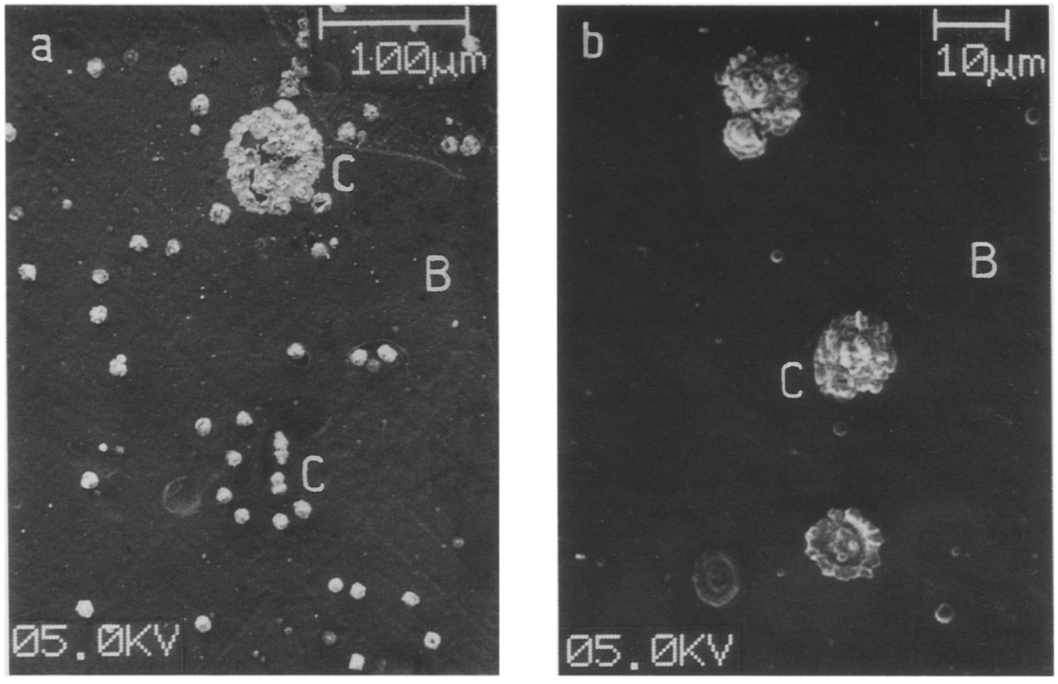

FIG 6. SEM photograph of the Pt/γ-Al_2O_3 surface after oxidation. (a) 204× magnification and (b) 1000× magnification. The sample was exposed to the ambient air during the transfer from the UHV system to the microscope.

conditions (see below). Treatment in oxygen causes a shift of the Pt 4*f* levels of 1.8 eV toward higher binding energies. This state can be assigned to Pt^{2+} (*23, 24*). We note that after this oxidation almost complete conversion to the Pt^{2+} state occurs. An indirect observation of Pt in the 2+ state is reported from IR data (*12*). The existence of Pt^{4+} (*25*) cannot be excluded from our data but is hard to determine precisely because of the overlap with the Al 2*p* levels. After successive hydrogen treatment we observe a partial reduction of the oxidized state. The width of the Pt 4*f* levels increases considerably, indicating that both the metallic and oxidized states coexist. However, the large width of the levels indicates also that contributions with an oxidation state formally smaller than 2+ exist, indicative of a mixed Pt–Al oxide, a finding which is in agreement with Ref. (*12*). We note that the determination of the oxidation states of Pt is delicate and certainly not possible on powder samples as the fine structure and precise energy position of the Pt levels is overcome by the large FWHM usually obtained on samples suffering from inherent charging problems.

For the Mo-modified supports we note differences in the amount of Mo on the surface as determined by ISS, the amount of Mo in the bulk as detected by XPS, and the values determined from the concentration of the liquids used for impregnation. For example, after impregnation with 4.39% Mo (XPS), we find that the surface is covered with 8.65% Mo (ISS). Similar findings are observed for the different preparation states, as shown in Table 2. The reduced state has the highest Mo concentration on the surface, but the Al concentration has increased, too; we obtain in this case the largest metal-atom concentration. In general, the extremely surface-sensitive ISS

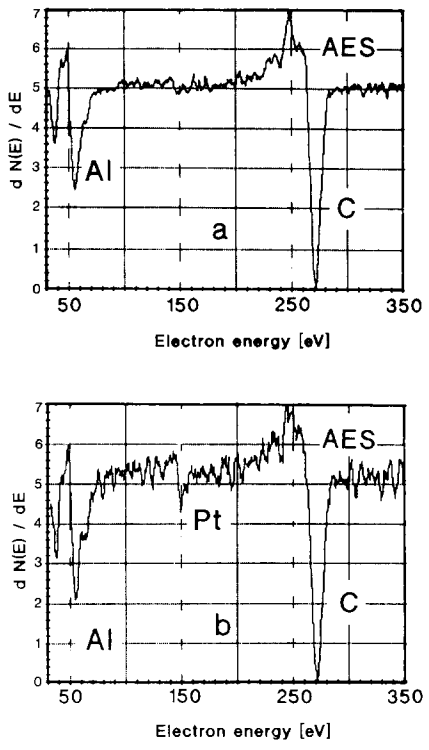

FIG. 7. Local Auger spectra (primary beam diameter 500 Å) of (a) background (B), (b) a Pt cluster (C) of sample shown in Fig. 6.

data show a larger molybdenum concentration, compared with the more bulk-sensitive XPS results. However, the atomic percentages determined from XPS also are rarely in line with those determined from the concentrations of the solutions used. These observations indicate that the dopants are preferentially adsorbed in the surface near regions and also give strong evidence for clustering and selective interactions among the dopants themselves.

An analysis of the relative Al and Mo concentrations is given in Fig. 9. Here we use the total quantities of the Mo 3*d* signal compared to that of the Al 2*p* signal. For increasing Mo concentrations the amount of Al detected in the XPS signal is plotted for the oxidized, reduced, and sulfided MoO_3/γ-Al_2O_3 films. This analysis is only valid assuming charge neutrality as well as a constant activity of oxygen (sulfur) at all Mo concentrations. The latter requirement implies that there are no changes in the oxygen (sulfur) oxidation state, for example due to formation or diffusion of OH groups. Under these conditions we expect a linear relation between the total amounts of Mo and Al. Deviations indicate either changes in the oxidation state of Mo or changes in the stoichiometry of the mixed Mo–Al oxide. At low Mo concentrations the linear relation indicates that there is no clustering of Mo-oxides, but a homogeneous distribution in the volume detected by XPS.

For the oxidized state, for all concentrations of Mo investigated, the data are indeed on a straight line with a slope of $-5/4$. This behavior indicates that the incorporation of Mo forms a chemical compound in the near surface region which has an average stoichiometry of five Al^{3+} to four Mo^{6+} ions.

In the reduced state the Al concentration

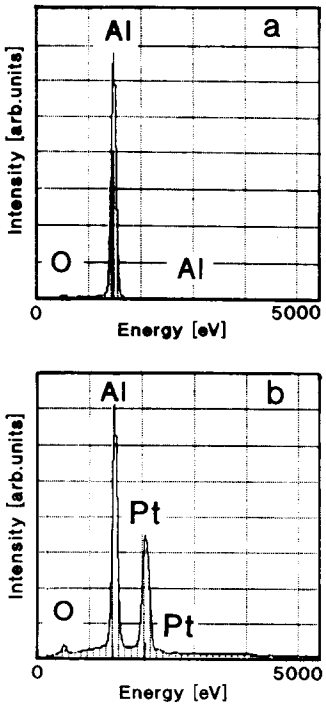

FIG. 8. Corresponding EDX spectra of the (a) background (A) and (b) a Pt cluster (B) of the sample shown in Fig. 6.

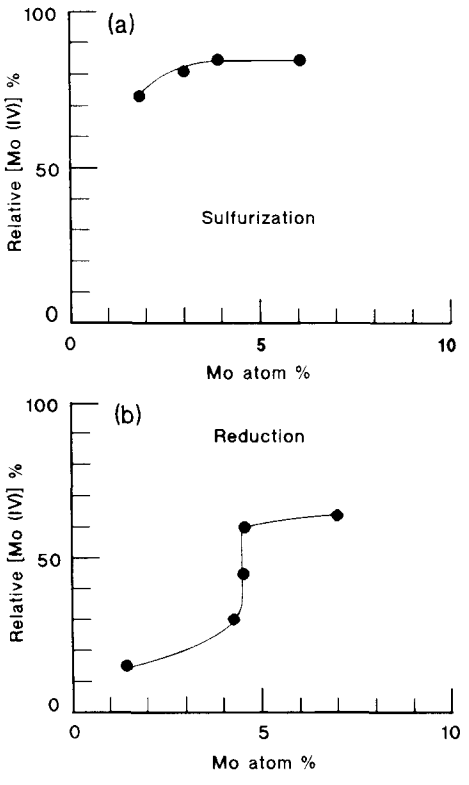

FIG. 9. Al concentration versus that of Mo (atomic percentages) in all chemically modified states of the system MoO_x/γ-Al_2O_3.

follows the straight line but above 4% Mo it increases from 33.5% to 37%. This deviation can be explained by either a change in the average oxidation state or in a change in stoichiometry. The latter might be explained by surface agglomeration of molybdenum as a consequence of the reducing treatments.

A similar behavior is observed for the sulfided state. The ratio is consistent with clusters consisting of MoS_2 and $MoOS_x$ to form a defect-rich surface. An independent determination of the surface structure in this state is given by a comparison of the binding energies. Our value of 229.8 eV (E_B^F) is close to that observed in cleaved MoS_2 (229.4 eV) (*26*). Formation of MoS_2 is also established by EXAFS and Raman results (*27, 28*). Unfortunately, our experimental methods are not suited to the determination of the size of the MoS_2 clusters at the MoO_3/γ-Al_2O_3 surface.

Further analysis considers the contribution of the different binding states of Mo for different Mo concentrations. In general, core-level shifts are assigned to changes in the electronegativities (Pauling term), in the ionicities (Madelung term) and in the final states (relaxation term) in the environment of the photoionized atom. For the Mo/γ-Al_2O_3 interaction all terms are expected to contribute to the resulting shifts and a separation a priori is not possible. Such contributions include variations of the oxidation state of the Mo ion, the different next-neighbor interactions in the various possible coordinations (*29*), the activity changes in the γ-Al_2O_3 ionic crystal, and its screening mechanism as an insulating material. The latter has been reported for oxidized W and Ta foils (*30*). The core-level shifts of Ta^{5+} and W^{6+} (referred to the metallic signal) are 4.9–5.5 eV and 3.9–4.5 eV, respectively. For the system Mo/γ-Al_2O_3, in the literature there is some work on different oxidation states of Mo, which includes the completely oxidized 6+ state (*5, 31, 32*). This value has a strong contribution from relaxational screening in the oxide and hence is expected to be larger than on oxidized metal surfaces. The intermediate states of Mo(5+) (*32, 33*) and Mo(4+) (*34*) are also observed, although the absolute values for these oxidation states depend on the charging and reference level used and hence differ within 1 eV (*17*).

In our work, we can determine the core-level shifts more precisely and use these assignments to determine the binding state of Mo. The Al 2*p* levels of clean metallic aluminum can be used as a reference signal for the interaction between molybdenum oxide and γ-Al_2O_3. However, for the discussion of core-level shifts it is more appropriate to refer the levels to the valence band maximum of γ-Al_2O_3 (E_B^V); for bare γ-Al_2O_3 surfaces it is found 5.6 eV below E_F. The reason for using E_B^V is demonstrated for the spectra obtained after the impregnation of

γ-Al_2O_3 by Mo solutions. The Al 2*p* level in bare γ-Al_2O_3 is shifted for 3.6 eV and after the impregnation the shift is reduced from 3.6 to 3.0 eV, whereas the metallic signal does not shift. This behavior is not due to a chemical change in the Al but is due to a Mo-induced change in the work function (E_F-E_V), as determined independently from UPS data (*14*). Variations in (E_F-E_V) are due to migration of defects within the γ-Al_2O_3 films. The use of E_B^V instead of E_B^F separates the work function changes from the chemical variations and therefore must be used for reliable evaluations. At this point it should be mentioned that a precise determination of both work function and chemical shift is impossible in data obscured by charging. The change in the work function is reflected also in the Mo 3*d* spectra. A complete list of the observed energy positions is given in Table 1; we have included both the values with respect to E_F (E_B^F) and with respect to E_V (E_B^V). In the following section we concentrate on the variations that occur in the binding energies of the Mo 3*d* levels and follow the changes in their oxidation states after the various chemical modifications and for different Mo concentrations.

It should be mentioned that the ability to distinguish different oxidation states of Mo is not directly correlated with determining the coordination of the Mo ions, and hence the kind of defect which is occupied. Mo^{4+} is known to exist only in six-fold coordination (0.65 Å); however, Mo^{5+} is a stable ion in four-fold (0.46 Å) and in six-fold (0.61 Å) coordination. Mo^{6+}, finally, is stable in the four-fold (0.41 Å), five-fold (0.5 Å), six-fold (0.59 Å), and seven-fold (0.73 Å) coordinations (*35*). The ionic radii for the differently coordinated Mo ions are given in brackets.

After the impregnation of γ-Al_2O_3 films by aqueous ammonium heptamolybdate solution one might expect to find Mo in the VI oxidation state. There are two possibilities for the chemical compound formed after the impregnation; a molybdenum oxide (*36*) or a molybdate $Al_2(MoO_4)_3$ (*37*). However, the binding energy of Mo $3d_{5/2}$ is 227.7 eV (233.1 eV) after the impregnation, a value which corresponds to Mo^{5+}. This reduced value could be caused by the significant contributions of the Madelung and relaxation terms of the ionic environment of γ-Al_2O_3. The increased FWHM in the initial impregnation may be caused by surface inhomogeneities or reflect adsorption of MoO_3 in different defect sites of the γ-Al_2O_3.

After the oxidation, the modified system definitely forms MoO_3/γ-Al_2O_3 (*31*) with Mo in the 6+ state. This becomes clear as we observe only a single, very sharp structure for all Mo concentrations. The binding energy of the Mo $3d_{5/2}$ level is 228.7 eV (235.8 eV) and the core-level shift with respect to the corresponding metallic signal is 6.35 eV. There is no charging as we observe no shifts in the Al 2*p* and O 1*s* levels. The assignment of the valence 6+, i.e., Mo(VI), to this state is in agreement with other authors (*5*, *31*, *32*). The sharpening of the emission indicates that there is only a single defect site in which Mo preferentially is to react. The surface structure of MoO_3/γ-Al_2O_3 within the two first monolayers is determined by the two configurations of aluminum in the spinel structure: Accordingly, the coordination of V_{Al}''' defects is either tetrahedral or octahedral. The chemical modification with Mo is found to maintain the γ-Al_2O_3 structure as demonstrated by the XPS core-level shifts and the TEM diffraction patterns. This is possible by a simple replacement of Mo in V_{Al}''' defects, as the ionic radii of Al^{3+} and Mo^{6+} in the tetrahedral (0.39 and 0.41 Å) and octahedral (0.535 and 0.59 Å, respectively) configurations are similar (*35*).

In the successively prepared reduced state of MoO_3/γ-Al_2O_3 we find shifts of the Mo 3*d* core level to lower binding energies and a very broad emission pattern with a maximum at 227.6 eV (234.4 eV). The relative population in each binding state is computed and the results are given in Table 1. In spite of the reduced binding energies in comparison with the oxidized state, we must conclude that in the reduced state some amount of Mo(VI) is still existent, at least at low Mo concentrations. In Figs. 3D, 3E

the main emission (doublet I) is now at a binding energy of the Mo $3d_{5/2}$ levels at 226.7 eV (233.8 eV), which can be assigned to Mo(V), in agreement with NMR experiments (*38*). Among the different possible oxidation states of Mo only the Mo^{5+} ion is paramagnetic. Curve II represents a different molybdenum species which according to its binding energy can be assigned to Mo(IV).

The sulfurization in H_2S has induced even more changes, as we observe a subsequent shift of the Mo $3d$ levels to lower binding energies. The lowest Mo $3d_{5/2}$ binding energy at a concentration of 6.22% is 222.5 eV (229.86 eV). At higher Mo concentrations the contribution of Mo(IV) is dominating against that of Mo(V). However, when compared with the reduced state the total amounts are significantly different; at all concentrations the Mo(IV) contribution dominates. The relative variations of the Mo(IV) and Mo(V) components are less pronounced and there is only a slight increase of the Mo(IV) contribution around 5% Mo.

We now discuss the assignment of Mo oxidation states, and next the occurrence of phase transitions in the reduced and sulfurized states. Regarding the binding energies of Mo $3d$ levels in the different states, we find a clear classification into three ranges, which allow a distinct assignment; i.e., the contribution of the Pauling term is dominating. The 6+ state appears at a defined binding energy, while the binding energies of the 5+ and 4+ states cover a range of about 1 eV. This behavior is indicative of different contributions from the Madelung and relaxation terms and not of discrete states that change their relative population. It reflects a continuous change from Mo(VI) states to Mo(IV) depending on the Mo concentration.

The total shift observed in the binding energy of the Mo $3d_{5/2}$ level is from 227.7 eV (234.7 eV) in the oxidation state (Mo^{6+}) to 222.4 eV (230.0 eV) in the reduced state (Mo^{4+}) at a concentration of 7.0%. The occupation of the tetrahedral and octahedral sites with Mo in the first and second monolayer can be determined from the separation of the Mo(V) and Mo(IV) components in the Mo $3d$ emission with increasing Mo concentration. To do this, we have calculated the relative contributions of Mo(IV) and Mo(V) states normalized to the total amount of Mo as a function of the Mo concentration. For this discussion we concentrate on the variations for the Mo(V) state, as displayed in Fig. 10. In the reduced state, we find that the Mo(V) contribution for initial concentrations (2.5%) is larger than that of Mo(IV). At 4.5% both curves cross in a small range of Mo concentrations and above 5% the Mo(IV) contribution dominates and is almost independent on the Mo concentration. These variations of the relative amounts of Mo(IV) and Mo(V) indicate a phase transition in the surface morphology for the reduced state. At low concentrations (below 2.5%) Mo is incorporated in the Mo(V) state as it finds octahedral and tetrahedral sites within the first monolayer. Above 2.5% the

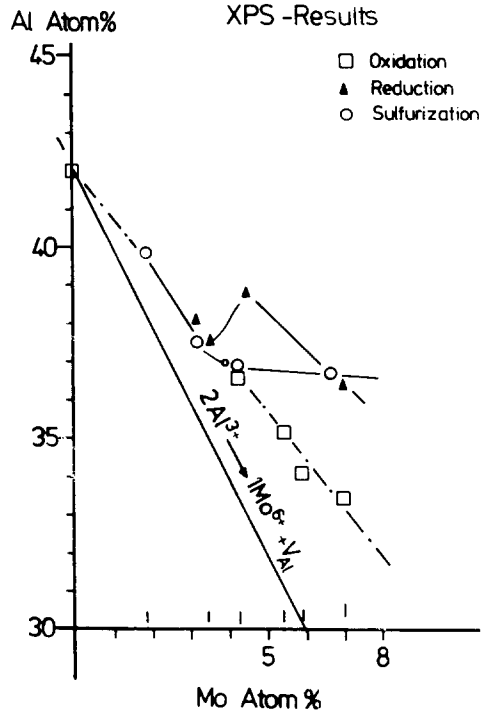

FIG. 10. Concentration-dependent variations of the Mo(IV) and Mo(V) relative populations determined from the relative intensities within the Mo $3d$ XPS lines.

Mo(IV) occupies the octahedral sites in the second monolayer. At 4.5% we find a critical change of the Mo(V)/Mo(IV) ratio. The Mo(IV) ion preferentially occupies the octahedral sites which are the most likely Al vacancies. Above 4.5% the Mo(IV) occupation of octahedral sites induced an excess charge and at 5% Mo the defects in the second layer will be occupied, thereby stabilizing a different phase. The strong change in the slope of the Mo(V) and Mo(IV) curves at 4.5% Mo (Fig. 10) indicates a phase transition from a homogeneously distributed MoO_x/γ-Al_2O_3 to the formation of MoO_2 clusters. This idea is supported by the Mo $3d_{5/2}$ binding energy (approx. 229.4 eV) of the probes with the largest Mo concentration, and on the observation of excess Mo in this state, demonstrated by the ISS results and the behavior in Fig. 10.

The relative parts of Mo(V) and Mo(IV) versus the total Mo concentration are shown in Fig. 10. It is possible to compare the results on MoO_3/γ-Al_2O_3 thin films in the reduced state with other studies (*5*). The crossing point of the curves at 4.5% Mo corresponds to a phase transition at 12% wt MoO_3 (*5*). Approximately 9% wt MoO_3 are found to cover the first monolayer of γ-Al_2O_3 (*5*) and at this concentration the catalyst shows the highest activity. Assuming a proportional relation to our films the first monolayer will be covered with 3.5% Mo atom percentage. We must consider in this case that the specific surface area ($\approx$1.5 m^2/g (*39*)) of our thin films is considerably lower than the specific area ($\approx$200 m^2/g) of powder catalyst and the porosity is avoided by thin films. Therefore, we expect the thin film surface to be covered by smaller amounts of MoO_3 compared to the powder catalyst. Impregnation below 4% of Mo is catalytically interesting but above 4.5% Mo atom concentration we observe formation of clusters. Clusters are known to be catalytically less active and only influence the selectivity of the catalyst.

Finally, our findings, derived by the accurate determination of binding energies of Mo 3*d* levels upon different chemical treatments, can be summarized in a consistent model which describes the preparation of an active catalyst:

A homogeneous oxidation of the surface of γ-Al_2O_3 by Mo is confirmed by the stability of the γ-phase, the similarity of the ionic radii in the fourfold and sixfold coordination, and the formation of Mo(VI) in the oxidized state. These findings are supported by the different amounts of Mo at the surface determined from the surface-sensitive technique ISS and from the bulk-sensitive XPS (see Table 2), and are in line with earlier models (*31, 40, 41*). In the reduced state the Mo 3*d* components arising from Mo(V) and Mo(IV) correspond to the formation of surface hydroxylation and oxygen vacancies, respectively (*42*). In the sulfurized state Mo–S bonds can be formed at oxygen vacancies thereby stabilizing a defect-rich surface with Mo in both the 4+ and by remaining OH groups also the 5+ states (*43*). A schematic view of the Mo/γ-Al_2O_3 surface in the different chemical modified states is given in Fig. 11.

We mention that the occurrence of phase transitions reflects itself also in the work function changes of the γ-Al_2O_3 films in the different modified states (*15*). We find for all states (oxidized, reduced, and sulfided) pronounced variations around Mo concentrations of 4.5%. This is a further, independent confirmation on the critical role of Mo which can ideally form perfectly aligned Mo–Al surface oxides, or at higher concentrations, can poison the surface by the formation of Mo clusters.

In summary, we identified in this study the oxidation states of Mo and Pt on chemically modified γ-Al_2O_3 supports as a function of concentration, temperature, and after oxidation, reduction, and sulfurization treatments. For the Pt/γ-Al_2O_3 system agglomeration of a mixed Pt-oxide with a mean oxidation state of Pt^{2+} is derived. For the Mo/γ-Al_2O_3 system a more detailed study gives new information on the surface morphology and defect structure. The data are

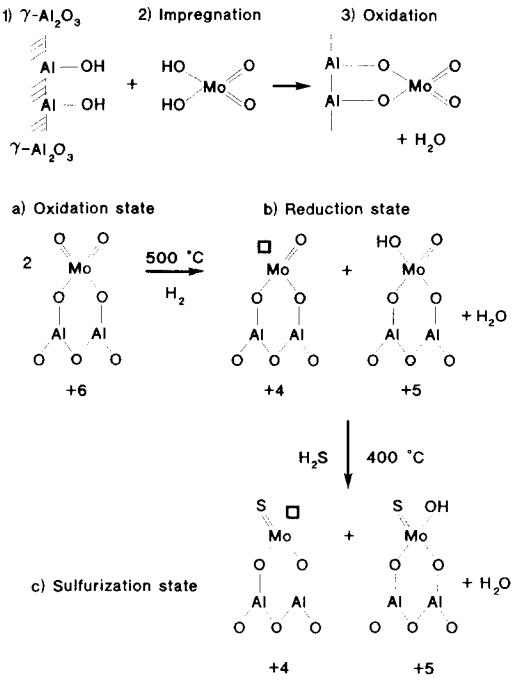

FIG. 11. Schematic model of the Mo/γ-Al_2O_3 surface in the different chemical modifications.

consistent with several findings derived from other techniques and from the chemical behavior of catalysts. However, a detailed analysis of the different oxidation states becomes possible by the use of photoelectron spectroscopy free of charging. Thereby, the correspondence to the catalytic activity becomes evident as the chemically stable states of Mo(VI) and Mo(IV) are not catalytically active; they can only influence the selectivity of the catalysts when present in large clusters. Active defects with Mo in the V and IV states are found predominantly at concentrations below 4% in the reduced and sulfurized states.

ACKNOWLEDGMENTS

We acknowledge the interest and support of Prof. W. Göpel, and we thank Prof. K. H. Herrmann for the use and performance of TEM facilities, H. Kohler (Conducta AG) for a critical reading of the manuscript and helpful comments, and B. Suhr and W. Neu for excellent experimental assistance. This work is supported in part by Degussa. A.J.G. acknowledges a grant from the Instituto Mexicano del Petroleo.

REFERENCES

1. Eiswirth, M., and Ertl, G., *Surf. Sci.* **177,** 90 (1986).
2. Dubois, L. H., Hansma, P. K., and Somorjai, G. A., *Appl. Surf. Sci.* **6,** 173 (1980).
3. Knözinger, H., and Ratnasamy, P., *Catal. Rev. Sci. Eng.* **17,** 31 (1978).
4. Taglauer, E., and Heiland, W., *Appl. Phys.* **9,** 261 (1976).
5. Zingg, D. S., Makovsky, L. E., Tischer, R. E., Brown, F. R., and Hercules, D. M., *J. Phys. Chem.* **84,** 2898 (1980).
6. Gates, B. C., Katzer, J. R., and Schuit, G. C. A., "Chemistry of Catalytic Processes." McGraw-Hill, New York, 1979.
7. de Beer, V. H. J., van Sint Fliet, T. H. M., Engelen, J. F., an Haandel, A. C., Wolfs, M. W. J., Amberg, C. H., and Schuit, G. C. A., *J. Catal.* **27,** 351 (1972).
8. Kasztelan, S., Grimblot, J. and Bonnelle, J. P., *J. Phys. Chem.* **91,** 503 (1987).
9. Lippens, B. C., and de Boer, J. H., *Acta Crystallogr.* **17,** 1312 (1964).
10. Löwe, A., and Hoffman, U., *Chem.-Ing. Tech.* **57,** 835 (1985).
11. Koberstein, E., and Völker, H., *Chem.-Ing. Tech.* **50,** 905 (1987).
12. Herz, R. K., and Shinouskis, E. J., *Appl. Surf. Sci.* **19,** 373 (1984).
13. Jiménez-González, A., and Schmeisser, D., *Surf. Sci.*, in press.
14. Jiménez-González, A., and Schmeisser, D., submitted for publication.
15. Rager, A., Gompf, B., Dürselen, L., Mockert, H., Schmeisser, D., and Göpel, W., *J. Mol. Electron.* **5,** 227 (1989).
16. Mockert, H., Schmeisser, D., and Göpel, W., *Sens. Actuators* **19,** 159 (1989).
17. These values appear 0.4 eV at higher binding energies when compared with Williams, G. P., "Electron Binding Energies of the Elements." Brookhaven BNSL, Upton, NY, 1983.
18. Briggs, D., and Seah, M. P., "Practical Surface Analysis." Wiley, New York, 1983.
19. Flodström, S. A., Petersson, L. G., and Hagström, S. B. M., *J. Vac. Sci. Technol.* **13,** 280 (1976).
20. Flodström, S. A., Bachrach, R. Z., Bauer, R. S., and Hagström, S. B. M., *Phys. Rev. Lett.* **37,** 1282 (1976).
21. Flodström, S. A., Martinson, C. W. B., Bachrach, R. Z., and Bauer, R. S., *Phys. Rev. Lett.* **40,** 907 (1978).
22. Bachrach, R. Z., Flodström, S. A., Bauer, R. S., Hagström, S. B. M., and Chadi, D. J., *J. Vac. Sci. Technol.* **15,** 488 (1978).
22. Cooke, D. L., Thomson, E. D., and Merrill, R. P., *Catal. Rev. Eng.* **26,** 163 (1984).
23. Kim, K. S., Winograd, N., and Davis, R. E., *J. Am. Chem. Soc.* **93,** 6296 (1971).

24. Peuckert, M., and Bonzel, H. P., *Surf. Sci.* **145,** 239 (1984).
25. Pirug, G., Dziembaj, R., and Bonzel, H. P., *Surf. Sci.* **221,** 553 (1989).
26. Jaegermann, W., and Schmeisser, D., *Surf. Sci.* **165,** 143 (1986).
27. Zmierckzak, W., Quader, Q., and Massoth, F. E., *J. Catal.* **106,** 65 (1987).
28. Clausen, B. S., Topsøe, Candia, R., Villadensen, J., Lengeler, B., Als-Nielsen, J., and Christensen, F. J., *J. Phys. Chem.* **85,** 3868 (1981).
29. Kohler, H., Neu, W., Kreuer, K. D., Schmeisser, D., and Göpel, W., *Electrochem. Acta* **34,** 1755 (1989); Kohler, H., and Göpel, W., in preparation.
30. Himpsel, F. J., Morar, J. F., McFeely, F. R., Pollack, R. A., and Hollinger, G., *Phys. Rev. B* **30,** 7236 (1984).
31. Giordano, N., Bart, J. C. J., Vaghi, A., Castellan, A., and Martinotti, G., *J. Catal.* **36,** 81 (1975).
32. Jiménez-González, A., MS thesis, Instituto Politecnico Nacional, Mexico D.F., 1982.
33. Patterson, T. A., Carver, J. C., Leyden, D. E., and Hercules, D. M., *J. Phys. Chem.* **80,** 1700 (1976).
34. Kim, K. S., Baitinger, W. E., Amy, J. W., and Winograd, N., *J. Electron Spectrosc. Relat. Phenom.* **5,** 351 (1974).
35. Shannon, R. D., *Acta Crystallogr. Sect. A* **32,** 751 (1976).
36. Holleman and Wiberg, E., "Lehrbuch der Anorganischen Chemie." de Gruyter, Berlin, 1976; Jezirowski, H., and Knözinger, H., *J. Phys. Chem.* **83,** 1166 (1979).
37. Brown, F. R., Makovsky, L. E., and Rhee, K. H., *J. Catal.* **50,** 385 (1977).
38. Seshadri, K. S., Massoth, F. E., and Petrakis, L., *J. Catal.* **19,** 95 (1970).
39. Hönicke, D., *Appl. Catal.* **5,** 179 (1983).
40. Dufaux, M., Che, M., and Naccache, C., *C. R. Acad. Sci. Paris, Ser. C* **268,** 2255 (1969).
41. Schuit, G. C., and Gates, B. C. *AIChE J.* **19,** 417 (1973).
42. Massoth, F. E., *J. Catal.* **30,** 204 (1973).
43. Massoth, F. E., *J. Catal.* **36,** 164 (1975).